CrossMark

ORIGINAL ARTICLE

The Electrochemical Dissolution of Noble Metals in Alkaline Media

Maximilian Schalenbach[1] · Olga Kasian[1] · Marc Ledendecker[1] · Florian D. Speck[1,2] ·
Andrea M. Mingers[1] · Karl J. J. Mayrhofer[1,2,3] · Serhiy Cherevko[1,2] (iD)

Abstract In this study, the electrochemical transient dissolution of polycrystalline silver, gold, iridium, palladium, platinum, rhodium, and ruthenium is examined in 0.05 M NaOH alkaline electrolyte as a function of electrode potential. An inductively coupled plasma mass spectrometer connected to an electrochemical flow cell is used for online detection of the metals dissolution rates. Broad potential windows starting from the hydrogen and going to the oxygen evolution reaction (OER) potentials are used to study the dissolution. The measured dissolution data, such as onsets of dissolution are analyzed and compared with available thermodynamic data. For most metals, at potentials, at which thermodynamics predict metal/solute or metal/oxide transitions, an initiation of the dissolution process is observed. It is suggested that dissolution during metal/oxide transitions is a purely kinetic effect that reflects the solubility of unstable transient oxides. Such oxides can also be formed during the oxygen evolution reaction. The latter fact is used to explain metals dissolution in the region of OER.

✉ Maximilian Schalenbach
m.schalenbach@mpie.de

✉ Serhiy Cherevko
s.cherevko@fz-juelich.de

1   Department of Interface Chemistry and Surface Engineering,
    Max-Planck-Institut für Eisenforschung GmbH, Max-Planck-Strasse
    1, 40237 Düsseldorf, Germany

2   Helmholtz-Institute Erlangen-Nürnberg for Renewable Energy
    (IEK-11), Forschungszentrum Jülich GmbH, Egerlandstr. 3,
    91058 Erlangen, Germany

3   Department of Chemical and Biological Engineering,
    Friedrich-Alexander-Universität Erlangen-Nürnberg, Egerlandstr. 3,
    91058 Erlangen, Germany

Introduction

Noble metals are well-known for their application in electrochemical devices such as fuel cells [1], electrolysers [2], and related systems. The use of these expensive precious metals is justified by their superior catalytic properties towards the oxygen reduction and evolution reaction (commonly abbreviated as ORR and OER) [3, 4] or hydrogen oxidation and evolution reaction (HOR and HER) [5, 6]. In alkaline media, non-noble metals such as Ni and Co can be employed as catalysts for these reactions as their stability is sufficiently high [7, 8]. Nevertheless, noble metals are predominantly used as HER, HOR, and ORR catalysts owing to their higher electrochemical activity [9]. The alkaline OER is an exception, as it is typically conducted by using non-noble oxidized metal catalysts such as nickel, cobalt, and iron [2]. However, as non-noble metals do not enable an efficient catalysis of the ORR, noble metals are considered to realize reversible oxygen electrodes for devices such as reversible fuel cells or batteries with air electrodes. With relevance to these applications, the stability of noble metals towards the oxygen reactions is of pivotal importance.

Recently, detailed experimental data on the time- and potential-resolved electrochemical dissolution of noble metals in acidic electrolyte have been reported by several groups [10–14]. With help of these data a direct comparison of electrochemical stability of the noble metals in acidic electrolyte

became feasible. Thus, for example, it was shown that despite of differences in affinity to oxygen (nobility), Ru and Au dissolve in a similar way during the acidic OER [10]. The latter was attributed to similarities in the OER mechanisms on these metals. As for alkaline electrolytes, however, such comparisons are fairly possible, as the existing data on their dissolution in this media is scarce and incoherent [7, 15–18]. As a starting point, available thermodynamic data can be used.

The summarized thermodynamic data on electrochemical equilibria of metals in aqueous solutions can be found in the "Atlas of electrochemical equilibria in aqueous solutions" of Pourbaix et al. [19]. Using these data, potentials at which dissolution of a noble metal at a given pH may be initiated can be found. Unfortunately, the available data for noble metal dissolution in the alkaline range of pH is not complete. As an example, thermodynamically Pt is stable in base, while it was experimentally measured that Pt dissolves (kinetics effects cannot be excluded though [15]). The real onset of measurable dissolution and potential dependence of dissolution rates are controlled by kinetics and cannot be acquired from the Pourbaix diagrams. Moreover, the OER on the surface of noble metals leads to continuous variation of the oxidation state of metal cations, which means that the states predicted by thermodynamics are not representative in this case. Thus, experimental measurements of dissolution rates are essential to verify the thermodynamic data and further describe the kinetics of dissolution processes.

This work aims to fill this lack of information on the stability of noble metals in alkaline electrolyte by collecting experimental data. In this focus, metal dissolution in the water stability region and during the OER potentials was addressed. For this purpose, the potential dependent dissolution rates of noble metals in aqueous 0.05 M sodium hydroxide solution were precisely quantified using a setup based on an electrochemical scanning flow cell coupled to an inductively coupled plasma mass spectrometer (SFC-ICP-MS) [20].

Experimental Section

Dissolution rates of Ag, Au, Ir, Pd, Pt, Rh, and Ru were measured by employing a setup that was developed in our group. For technical details please refer to our previous publications [20, 21]. In short, the setup consists of a three-electrode electrochemical scanning flow cell (SFC) directly connected to an inductively coupled plasma mass spectrometer (ICP-MS, Perkin Elmer, Nexion 350X). The measured samples consisted of commercially available discs (Mateck, Germany) with purities of at least 99.9%. The samples were freshly polished (with alumina particles down to 0.3 μm) before each measurement. During the measurements, the samples were in contact with an argon purged 0.05 M NaOH (Merck, Suprapur, purity > 99.99%) solution, which

corresponds to a pH of approximately 12.7. The electrolyte was directed through the cell with a flow rate of approximately 3.3 μl s^{-1}. A sample area of approximately 1.2×10^{-2} cm^2 was exposed to the electrolyte. An Ag/AgCl reference electrode (Metrohm) with a 3 M KCl solution was used to measure the potential at the examined metals. In order to avoid any contacts of the working electrode with chloride ions from the reference electrode, the latter is positioned in the outlet channel of the SFC. The potentials that are stated in this article refer to the reversible hydrogen electrode (RHE) as reference and were calculated by deducting −0.21 V vs. NHE for the Ag/AgCl reference electrode and −0.71 V for the pH shift. Delays that arise from the transport of the electrolyte from the electrochemical flow cell to the ICP-MS were subtracted in order to directly correlate potential and dissolution data.

Solutions of 0.5, 1, and 5 ppb of the measured metals were used to calibrate the ICP-MS. After passing the electrochemical cell and before entering the ICP-MS, the alkaline electrolyte was acidified with an aqueous solution of 0.1 M HNO$_3$ (Merck, Suprapur, purity > 99.99%) using a Y-connector with a one to one mixing ratio. To ensure that a possible ICP-MS performance change does not influence experimental results, internal standard solutions were mixed to the acidic solution to control the ICP-MS measurement. For this purpose, concentrations of 7.5 ppb Rh for Ag, Pd, and Ru; 10 ppb Re for Au, Ir, and Pt; and 50 ppb Ge for Rh were used. Detections limits of the ICP-MS setup were determined (as commonly conducted in the community) by calculation of the standard deviation of the signal from the blank alkaline electrolyte and multiplying it by three.

Two different protocols were applied to measure dissolution rates: (i) cyclic voltammetry with two periods between 0.05 and 1.5 V vs. RHE and (ii) linear sweep voltammetry starting from 1.2 V vs. RHE until a current density of 4 mA cm^{-2} was reached. Both protocols were conducted with scan rates of 0.002 V s^{-1}. In the case of the first protocol, potentials of 0.1 V vs. RHE were applied for 10 min in order to reduce native oxide layers from the metal samples. In the case of the second protocol, a voltage of 1.2 V was applied for 10 min before the potential sweep was started in order to oxidize the polished samples. All measurements were repeated at least 2–3 times in order to ensure reproducibility of the obtained data. The deviations between the repetitions of the measured absolute values of the potential dependent dissolution rates were below 30% for each metal.

Results

Noble Metal Dissolution in the 0.05 and 1.5 V Potential Range

To estimate the stability of the examined noble metals, the applied potentials roughly ranged in the electrochemical water

stability window (except for the highly active Ru). Accordingly, two cycling voltammograms (CVs) with a scan rate of 0.002 V s^{-1} were recorded between 0.05 and 1.5 V. Figure 1 shows the corresponding potential- and time-dependent change of Ag, Au, Pd, Pt, Ir, Rh, and Ru dissolution rates during this potential excursion. The dissolution rate is displayed as the mass change *dm* in the units of nanograms normalized to the geometric surface area *A* of the samples in

square centimeters and the time *t* in seconds. In addition to the experimental results, vertical lines corresponding to the potentials of the phase transitions in thermodynamic equilibria [19] were also graphed. These potentials depend on the concentration of dissolved metal ions. According to this behavior, the following considerations were taken into account.

The detection limit of the ICP-MS can be used to estimate the concentration of the dissolved species on the electrode in the beginning of dissolution. The sensitivity of the ICP-MS is different for the studied noble metals, which must be taken into account. This was done by measuring the standard deviation of the ICP-MS signal from the electrolyte. In the case of the used cell, the concentration of dissolved metal ions directly at the electrode was previously reported to be approximately 100 times higher than that in the bulk electrolyte [22]. Hence, the measured concentration at the detection limit multiplied by 100 is the electrode concentration at the onset of the anodic dissolution (dissolution during the upper going potential sweep). The latter is further used in the Nernst equation (local equilibrium at the electrode is assumed) to get the thermodynamic potential. As for the cathodic dissolution, it is typical that there is still a tailing from the anodic dissolution, which must be taken into account. This was done by measuring the concentration on the onset of cathodic dissolution. Similarly to anodic dissolution, a factor of 100 was applied to obtain the concentration at the electrode out of the measured bulk concentration (see detailed description below). In the following, c_{up} and c_{down} denote the obtained concentration at the phase transition during the up-scan and down-scan, respectively. The values are summarized in Table 1.

Figure 2 depicts E vs. pH diagrams with respect to c_{up} and c_{down} measured in the current work. Unfortunately, as follows from the figure, data for solid-liquid transitions for the alkaline range of pHs were reported only for Ag, Au, Ir, and Ru [19]. In the case of Pd, Pt, and Rh, only thermodynamic data for solid to solid transitions (such as metal to oxide or oxide to higher/lower oxide) are reported. As follows from the results in Fig. 1, in most cases, these transitions matched well the onsets of dissolution. This latter finding indicates a correlation between metal oxidation to oxides/hydroxides and dissolution, also numerously reported for acidic electrolytes [10, 21].

As a metric for this correlation between available thermodynamic data and measured dissolution results, the difference between potentials of dissolution and phase transition was introduced, which is denoted as ΔE. For this purpose, the onset potential E_{onset}^{exp} of the dissolution (where 'exp' states for the experimentally obtained values) was extracted from the measured data. To do so, the data in Fig. 1 was graphed in a semi-logarithmic plot (see supporting information to this article provided online) and the onset potentials of the dissolution peaks were red out. The differences between the onset potentials and the thermodynamic potentials of the related phase transitions (taking the concentration for dissolved species from Table 1) are herein denoted as ΔE.
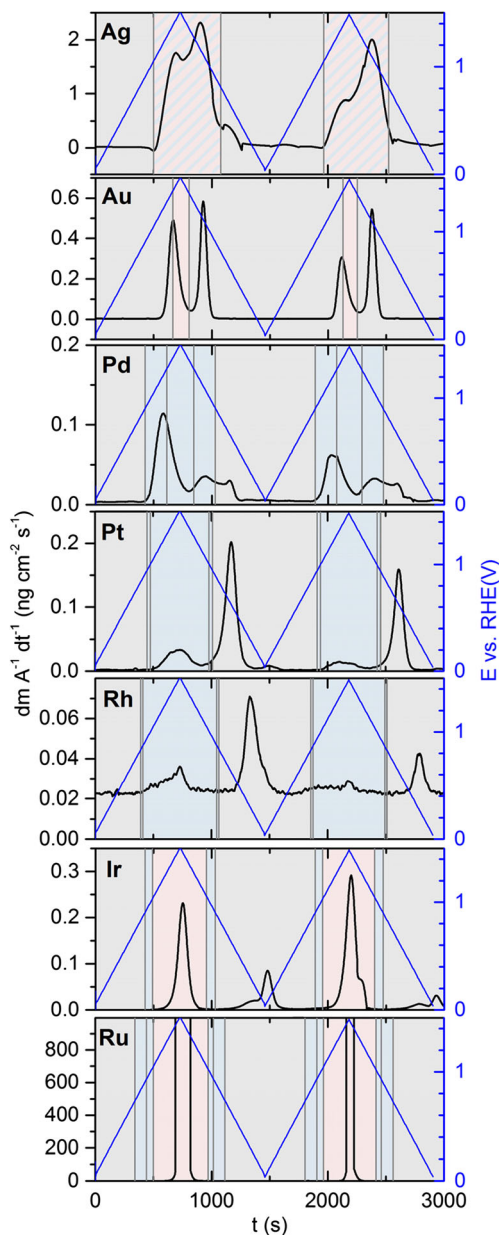

Fig. 1 Potential (right, blue axis) and dissolution rate of the metals (left, black axis) during cyclic voltammetry with a scan rate of 0.002 V s^{-1} as a function of time. Vertical gray lines: thermodynamically predicted phase transitions with reference to the measured concentrations of dissolved metal ions in the electrolyte. Grayish shaded areas: expected thermodynamic immunity against corrosion. Blue shaded area: expected formation of stable oxides. Reddish marked area: expected dissolution

Table 1 Summary of the phase transitions considered in this work including the thermodynamic potentials (E_{up}^{th} and E_{down}^{th}) extracted from the equations reported by Pourbaix et al. [19], the experimentally determined onset potentials of the dissolution (E_{up}^{exp} and E_{down}^{exp}), and the potential differences ΔE_{up} and ΔE_{down}. The concentration c_{up} represents the minimal detectable concentration at the electrode, while c_{down} represents the concentration at the electrode during the onset of the cathodic dissolution peak. a) A related dissolution peak is not visible. For example, the dissolution signal of a previous phase transition overshadows any further onset. In this case and a solid-liquid phase transition, E^{th} cannot be calculated as c_{up} or c_{down} is unknown. b) Two cathodic peaks occurred, which could not be unambiguously attributed to a phase transition. c) The oxide transitions were so close to one another that their mean value was considered

Metal	Phase transition		Up-scan				Down-scan			
	Lower oxidation state	Higher oxidation state	c_{up} (nM)	E_{up}^{th} @ c_{up} (V)	E_{up}^{exp} (V)	ΔE_{up} (V)	c_{down} (nM)	E_{down}^{th} @ c_{down} (V)	E_{down}^{exp} (V)	ΔE_{down} (V)
Ag	Ag	AgO^-	93	1.05	1.05	0.00	a	a	a	a
	AgO^-	Ag_2O_3	a	a	a	a	7310	1.41	1.43	0.02
Au	Au	$H_2AuO_3^-$	2.9	1.38	1.08	−0.30	153	1.41	1.29	−0.12
Pd	Pd	PdO	16	0.90	0.84	−0.05	121	0.90	0.73	−0.17
	PdO	PdO_2	a	1.28	a	a	184	1.28	1.35	0.07
Pt	Pt	PtO	1.4	0.98	0.91	−0.07	15 and 30b	0.98	0.12	b
	PtO	PtO_2	a	1.05	a	a	a	1.05	1.13	b
Rh	Rh	Rh_2O	21	0.80	0.87c	0.03c	15c	0.80	0.53c	−0.31c
	Rh_2O	Rh_2O_3	a	0.88				0.88		
Ir	Ir	IrO_2	0.6	0.93	0.83	−0.10	8 and 80b	0.93	0.14	b
	IrO_2	IrO_4^{2-}	a	1.03	a	a	a	1.10	0.90	b
Ru	Ru	Ru_2O_3	82	0.74	0.94	0.2	a	0.74	a	a
	Ru_2O_3	RuO_2	a	0.94			a	0.94	a	a
	RuO_2	RuO_4^-	a	a	a	a	a	1.04	a	a

In the case of the up-scan, ΔE_{up} is defined as

$$\Delta E_{up} = E_{up}^{exp} - E_{up}^{th} \qquad (1)$$

where E_{up}^{exp} and E_{up}^{th} denote the onset of a measureable dissolution and the thermodynamic potential of the phase transition, respectively. As described above, the detection limit served as a measure to calculate the reference concentration for E_{up}^{exp}.

In the case of the down-scan, the E_{down}^{exp} was calculated as

$$\Delta E_{down} = E_{down}^{exp} - E_{down}^{th} \qquad (2)$$

where E_{down}^{exp} and E_{down}^{th} denote the onset potential of the cathodic dissolution process and the thermodynamic potential for a reductive phase transition, respectively.

As described above, during the up-scan, some amount of metal was dissolved. Thus, during the down-scan, the concentration of dissolved ions was typically significantly higher than the initial values during the up-scan. To take this into account, the dissolution rate at the onset of the cathodic dissolution peak was measured, and the obtained value was converted to a concentration, respectively. Here, it is assumed that the species dissolved in up- and down-scans were identical. Further, by multiplying by a factor of 100 (with reference to the concentration difference described above) and employing

the concentration dependent equations reported by Pourbaix et al. [19], E_{down}^{th} was obtained.

Table 1 summarizes the estimated ΔE_{up} and ΔE_{down} of the dissolution. It is assumed that the obtained values were affected by an estimation error between 0.05 and 0.1 V. As follows from the table, during the up-scans, Pd, Pt, and Ir showed slightly lower, but still within the measurement accuracy, the same onset potentials as that predicted by thermodynamic data. A relatively high mismatch with $\Delta E_{up} = -0.3$ V was estimated for Au. This finding implies Au dissolution in the potential region where the thermodynamic data predicts immunity to corrosion. Dissolution of Ag, Rh, and Ru in the potential region where the thermodynamic data of Pourbaix et al. [19] predicts immunity during the up-scans was negligible/non-measurable. Excluding Rh, all metals show a distinct dissolution peak during the up-scans. During the down-scans, some metals showed significant dissolution signals in the potential range where immunity is expected. We attribute these dissolution features to the reduction of previously formed surface or subsurface oxides.

In the following, the measured dissolution features for each metal are discussed separately in detail, with respect to pH = 12.7 during the measurement. For this purpose, the thermodynamic data of Pourbaix et al. [19] are compared to the measured data. Since reported enthalpies for hydrated oxides and corresponding hydroxides, for example PtO × H_2O and Pt(OH)$_2$, are the same, only oxides are considered below in chemical

Fig. 2 Pourbaix diagrams for the electrochemical equilibria of the examined metals in aqueous non-complexing electrolyte. Solid-liquid phase transition in general depends on the amount of dissolved ions. The graphed relations refer to the stated concentrations in the graphs, which correspond to the detection limits of the experimental setups. Grayish shaded areas: immunity against corrosion. Blue shaded area: formation of stable oxides. Reddish marked area: dissolution
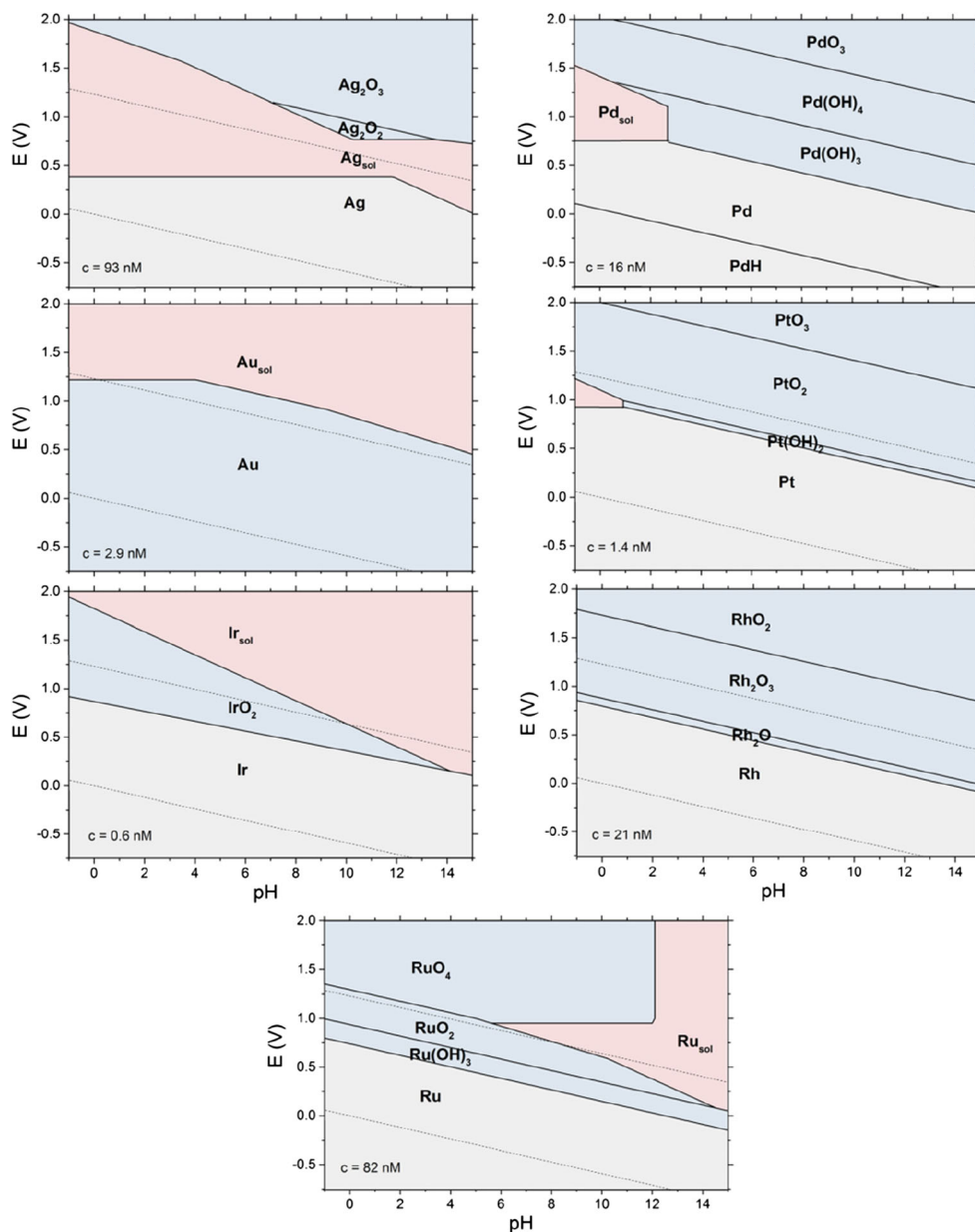
equilibria equations. Moreover, adopting the representation of Pourbaix et al., water is omitted in oxide's chemical formula.

Ag Based on the data collected by Pourbaix et al. [19], Ag belongs to those metals for which soluble species are thermodynamically predicted. Thus, as follows from $Ag + H_2O \rightarrow AgO^- + 2H^+ + e^-$, soluble AgO^- ions should be formed at anodic potentials higher than 1.05 V (here and below, the thermodynamically calculated potentials refer to the concentrations stated in Table 1). The amount of dissolved silver increases with potential. At even higher potentials, the reaction $2AgO^- + H_2O \rightarrow Ag_2O_3 + 2H^+ + 4e^-$ can lead to precipitation of AgO^- by the formation of stable Ag_2O_3. As the potential of this transition changes with concentration, no corresponding vertical line is given in Fig. 1.

According to the experimental data, a decrease in the dissolution rate at potentials close to $E = 1.4$ V forming a peak at the recorded mass-spectrogram can be assigned to this transition. The estimated ΔE_{up} for the Ag/AgO^- phase transition was zero, which points to a very good correlation between the thermodynamic and measured potentials and confirms that anodic dissolution is described by the discussed equations.

In the beginning of the down-scan, the concentration of silver ions (as estimated from the ICP-MS data) in the electrolyte was approximately 73 nM. Taking a factor of 100 into account for the estimation of the electrode concentration, the thermodynamically predicted reversible potential for the phase transition from AgO^- to Ag_2O_3 occurs at $E_{down} \approx 1.41$ V. This results in $\Delta E_{down} = 0.02$ V. Hence, the observed

dissolution peak can be explained by surface de-passivation due to reduction of Ag_2O_3 and that the same Ag/AgO^- dissolution process is now taking place during the down-going scan.

Au Like Ag, Au forms soluble species in the alkaline range of pH values. Following thermodynamic data [19], Au is supposed to be immune up to 1.38 V. At higher potentials the Au/Au^{3+} transition should take place as follows from the reaction $Au + 3 H_2O \rightarrow H_2AuO_3^- + 4H^+ + 3e^-$. However, our measurements indicate that Au already starts to dissolve anodically at approximately 1.08 V. This results in $\Delta E_{up} = -0.3$ V. While the origin of this deviation is not clear, hypotheses are elucidated in the 'discussion section' below. It should be noted that the initial increase in dissolution with potential is very sluggish. Hence, if a linear scale representation as in our previous work [15] is used, this initial increase is unnoticeable until an onset of ca. 1.2 V.

Even though it is not predicted thermodynamically, the formation of a stable oxide at higher potentials can be expected on the basis of the recorded data. Such an oxide could explain the observed decrease in the dissolution rate with potential, i.e., passivation. Similar to Ag, during the down-going scan, a dissolution peak initiates right after the potential vertex with $\Delta E_{down} = -0.12$ V. This peak might be attributed to a reduction of non-stable oxides that had been formed during the dissolution process. A more detailed discussion of Au dissolution in alkaline electrolyte is given in our previous work [15].

Pd Unlike Ag and Au, no soluble species in equilibrium with Pd or Pd hydrated oxide/hydroxide is reported in common Pourbaix diagrams. Hence, just the reported thermodynamic data for solid-solid transition in the form of $Pd + H_2O \rightarrow PdO + 2H^+ + 2e^-$ (expected at 0.9 V) and $PdO + H_2O \rightarrow PdO_2 + 2H^+ + 2e^-$ (expected at 1.28 V) could be considered in this work. Even though solid/soluble transitions were not considered in the thermodynamic data, significant dissolution was observed at the oxide transitions. During the up-scan, ΔE_{up} was estimated to be at around -0.05 V, which indicates that the observed dissolution may be related to the surface destabilization during the Pd to PdO transition. A small hump in the region of the PdO to PdO_2 transition, clearly seen during the second CV, could be attributed to an additional dissolution process triggered by this transition. During the down-scan, two Pd dissolution peaks with the onset potentials of 1.35 and 0.73 V were observed. The first peak matches the oxide transition from PdO_2 to PdO well. The origin of the second one could be attributed to the reduction of other oxides such as PdO.

Pt Similarly to Pd, two different stable oxidation states of Pt in the examined potential range with no dissolved species are expected. These transitions are described by $Pt + 2H_2O \rightarrow PtO + 2H^+ + 2e^-$ at 0.98 V and $PtO \rightarrow PtO_2 + 2H^+ + 2e^-$ at 1.05 V. Thermodynamics thus predicts a small potential

difference of 0.07 V between both oxide transitions. The onset of the anodic peak with $\Delta E_{up} = -0.07$ V corresponds well to the potential of the Pt to PtO transition. During the down-scan, two dissolution peaks with onset potentials of 1.13 and 0.12 V were observed. We assume that these peaks are attributable to the reduction of oxides; however, they cannot be unambiguously assigned to the oxide transitions, respectively. High stability of the oxides towards reduction and correlated kinetic barriers can explain the high potential differences between the onset of cathodic dissolution peaks and the thermodynamic potentials of the oxide transitions.

Rh Beside the fact that Rh is slightly less noble than Pt, both metals exhibit very similar stability in alkaline electrolyte. No stable soluble species are reported in common Pourbaix diagrams. Several solid-solid transitions are possible, as $2Rh + H_2O \rightarrow Rh_2O + 2H^+ + 2e^-$ at 0.8 V, $Rh_2O + H_2O \rightarrow 2RhO + 2H^+ + 2e^-$ at 0.88 V and $Rh_2O + 2H_2O \rightarrow Rh_2O_3 + 4H^+ + 4e^-$ at 0.87 V. During the up-scan, the dissolution peak at the first oxide transition is observed, although it is less distinct as in the case of the other metals. During the second sweep, this peak diminishes significantly. The obtained ΔE_{up} is close to zero, which indicates that a correlation between one of the oxidation processes and the observed dissolution is plausible. During the down-scan, a distinct dissolution peak can be observed. Depending on which oxide transition is used to calculate ΔE_{down}, values between -0.27 and -0.35 V can be obtained (c.f. Table 1).

Ir It is expected that Ir has one stable oxide phase between 0.93 and 1.03 V, as formed by $Ir + 2H_2O \rightarrow IrO_2 + 4H^+ + 4e^-$. Towards higher potentials, soluble species should be formed by $IrO_2 + 2H_2O \rightarrow IrO_4^{2-} + 4H^+ + 2e^-$ and their equilibrium concentration should increase with potential, which was also experimentally observed for the measured concentration. The obtained ΔE_{up} with respect to the first oxide transition is -0.1 V. During the down-scan, two peaks were observed with onset potentials of 0.90 and 0.14 V. Similar to Rh and the second cathodic dissolution peak of Pd and Pt, these peaks are attributed to strongly kinetically inhibited reduction of oxides.

Ru In the examined potential window, Ru can undergo two different solid-solid phase transitions, namely $2Ru + 3H_2O \rightarrow Ru_2O_3 + 6H^+ + 6e^-$ at 0.74 V and $Ru_2O_3 + H_2O \rightarrow 2RuO_2 + 2H^+ + 2e^-$ at 0.94 V. Similar to Ir, Ru does not form a thermodynamically stable oxide at high potentials, dissolving by $RuO_2 + 2H_2O \rightarrow RuO_4^{2-} + 4H^+ + 2e^-$. In this non-stable regime, Ru showed by far the highest dissolution rate of all measured metals. With reference to the high concentration of dissolved metal ions, we could not precisely track the extent of its dissolution between 1.4 and 1.5 V by using our measurement technique. Thus, the values for the dissolution are cut off

at dissolution rates exceeding 1 μg cm^{-2} s^{-1}. During the up-scan, a significant increase of the dissolution rate can be seen at approximately 0.94 V in the semi-logarithmic plot (see SI). It is questionable, whether this dissolution onset corresponds to the transition from Ru to Ru$_2$O$_3$ or from Ru$_2$O$_3$ to RuO$_2$. In the first case, $\Delta E_{up} = 0.2$ V is relatively high, while in the second case it is negligible. It can be suggested that either the first transition takes place without dissolution or it is kinetically strongly depressed so that it is delayed by 0.2 V. Further techniques have to be used to characterize this phase transition and the surface state in more detail. During the down-scan, we could not observe any distinct dissolution peak, which could mean that it was not possible to reduce the formed oxides in the measured potential range.

Dissolution during the OER

In acidic electrolyte, it has been shown that besides the dissolution during metal oxidation/reduction transition, also processes disturbing the surface oxide structure, such as the OER, affect the stability and may lead to dissolution [1]. Figure 3 presents similar data but now measured in alkaline electrolyte. Here, the dissolution rate and current density are plotted on the same potential scale during potential scans from 1.2 V towards potentials that correspond to currents of 4 mA/cm^2. As later discussed, the measured current is dominated by the OER. The activity of the metals towards the OER at 4 mA/cm^2 proceeds in the order Ru > Ir > Rh > Ag > Pd > Pt > Au, while the dissolution rate is decreasing in the order Ru > Ag > Au > Ir > Rh > Pt > Pd. Similarly to previously reported data by our group in acidic electrolyte [10], the general correlation between activity and stability of different noble metals, proposed recently [23], is not observed.

Figure 3 clearly shows that the dissolution rate increases with current and the accompanied OER. However, the Ag, Au, and Pd samples showed a peak in dissolution rate or current density approaching OER potentials. In the case of the Ag sample, a peak in current density was observed, which, however, did not lead to a remarkable feature in the dissolution rate. The onset of this peak was approximately at 1.51 V and thus could correspond to the transition from Ag$_2$O to Ag$_2$O$_3$. In the case of the Pd sample, the oxidation of PdO to PdO$_2$ occurs in thermodynamic equilibrium at 1.28 V (independent of the concentration of dissolved ions) and could be responsible for the observed Pd dissolution peak in Fig. 3. In this potential region, a distinct peak of Pd could not be observed in Fig. 1. It is likely that this peak was overshadowed by the dissolution peak of the first oxide transition. In the case of the Au sample, the origin of the dissolution peak before OER potentials was discussed above.

In order to estimate the relative stability of noble metals during the OER, the current efficiency of dissolution was estimated at a current density of 1 mA cm^{-2} as graphed in Fig. 4.
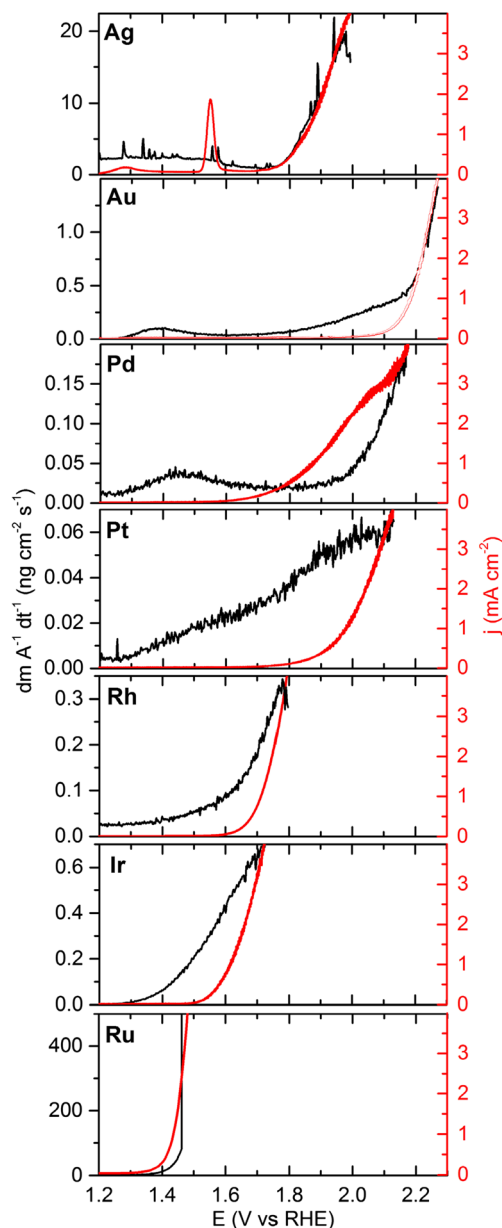

Fig. 3 Dissolution rates (left axis) and current densities (right axis) in the region of the oxygen evolution reaction. Data obtained during linear sweep voltammetry at a scan rate of 0.002 V s^{-1}

These current efficiencies were calculated by the ratio of metal dissolution current[1] and total measured current, respectively. In this study, similar to reports in acidic electrolyte, Ru is the least stable of the studied noble metals in the OER region. Surprisingly, Au showed two orders of magnitude lower dissolution current efficiency than Ru, although similar efficiencies were found for acidic OER [10]. This may be related to different mechanisms of acidic and alkaline OER on Au [15].

---

[1] The current corresponding to the dissolution rate was calculated on the basis of Faraday's law and the assumption that one electron was transferred in order to dissolve the oxide.
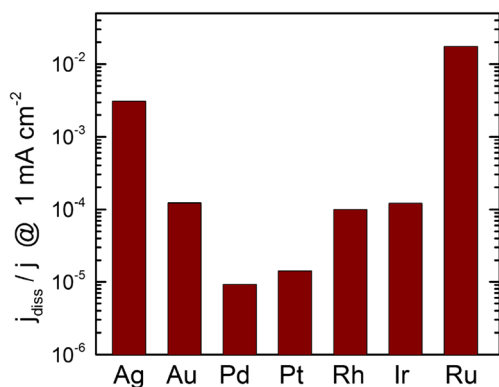
Fig. 4 Current efficiency of the dissolution as calculated by the ratio of the dissolution current to the overall current at 1 mA cm^{-2}

Dissolution efficiencies of Ir and Rh were comparable to Au, while the most stable noble metals in the OER region were Pt and Pd.

Discussion

Unlike for acids, thermodynamic data on noble metals in alkaline media are scarce. As an example, for Pd, Pt, and Rh, no dissolution at pHs > 7 is expected in the diagrams by Pourbaix et al. that are graphed in Fig. 2. However, as shown above, all noble metals dissolve to some extent in alkaline media. Hence, a short explanation on the applicability of thermodynamic data in interpreting experimental dissolution results should be given first.

The potentials and pHs of the phase transitions reported by Pourbaix et al. [19] refer to thermodynamic equilibria between the phases. These conditions imply a constant potential and pH as well as an infinite time to reach equilibrium. Depending on a chosen potential and pH, three cases can be defined in aqueous electrolytes: (a) if the potential is below the metal oxidation potential, the metal is expected to be immune against corrosion; (b) at higher potentials, it can be passivated/protected by formation of a stable oxide layer or (c) it dissolves. However, the presented measurements were conducted using CVs, where—due to the constant potential change—the electrode is neither in a thermodynamic equilibrium nor in a steady state. Hence, it is expected that kinetic effects become an issue. These kinetic effects can result in a shift between the potential where the phase transition is expected from thermodynamics and where the accompanied dissolution was actually measured. Depending on the time scale of the experiment and the intrinsic kinetic properties of the phase transition, the magnitude of this shift may vary.

Observed positive ΔE values in the solid/solute transitions for up-going scans and negative ΔE for the down-going scans can be attributed to kinetics. To address experimentally observed shifts in the opposite directions, several explanations can be given, such as (a) an additional phase transition which

is not reported in the thermodynamic data; (b) a wrong estimation of the phase transition's potential in the thermodynamic data; (c) high heterogeneity of the surface resulting in a broadening and dispersion of E_{up}^{th} and E_{down}^{th}; (d) the thermodynamic data is valid for bulk states, while the electrochemical reactions at the surface might be characterized by different potentials or reaction enthalpies than that during the electrochemical reactions at the surface. The latter two reasons can be used for explaining most deviations presented above. In general, also applicability of (a) and (b) is expected as the data reported by Pourbaix et al. [19] were extracted from old calorimetric measurements and often require revision, as recently discussed for Pt [21].

As discussed above for solid/solute transitions, the same reasoning can be used to explain deviations of measured and thermodynamic data on the solid/solid transitions. More important to discuss, however, is the apparent absence of thermodynamic data for dissolved species. Assuming that thermodynamic data are correct, the observed dissolution can be assigned to pure kinetic phenomena. Under the non-equilibrium conditions of a potential change between two stable phases, the metal goes through a series of intermediate phases. Some of these phases may have higher solubilities than the stable phases resulting in macroscopically observed dissolution [11]. As the measured system is not in equilibrium, escape and measurement of the dissolved species are possible. Thus, even if the initial and final state of a metal surface during a potential change are stable, an oxide transition between both states can lead to measurable dissolution. A representative example here is Pt. Oxide transitions such as Pt to PtO or PtO to PtO$_2$ coincide well with anodic and cathodic dissolution of Pt, which is a sign of some material destabilization leading to the observed transient dissolution. These dissolution processes are not in equilibrium with stable phases. Hence, they cannot be described by using stationary thermodynamic data.

During the non-equilibrium process of the OER, the oxidation states of metal catalysts are continuously changed. Accordingly, various oxidation states of the active metal components during the oxygen evolution were reported in the literature [24–30]. Binninger et al. [31] derived from thermodynamics that all metals may dissolve during the OER. Thus, even if thermodynamics predicts the formation of a stable oxide for OER potentials, the surface processes during the OER and correlated changes of the oxidation states lead to dissolution. Accordingly, the dissolution rate is a question of OER mechanisms and kinetics.

Summary

All noble metals studied in the current work dissolved in alkaline media. The extent of their potential dependent

dissolution was quantified using SFC-ICP-MS. A detailed analysis of the obtained experimental results and literature data on metal/oxide and/or metal/solute potential transitions was used to identify macroscopic processes responsible for the observed dissolution. It was shown that for most metals a good correlation between thermodynamic and measured data could be established. This agreement was reflected by relatively low values for ΔE (the potential difference between the onset of the dissolution peak and the thermodynamically predicted potential of the phase transition). This new finding reveals that despite the thermodynamically predicted stability, transitions of oxidation states and OER must be always taken into consideration for estimations of a noble metal's resistance towards corrosion in real applications.

References

1. J.-H. Jo, S.-C. Yi, J. Power Sources **84**, 87 (1999)
2. M. Schalenbach, G. Tjarks, M. Carmo, W. Lueke, M. Mueller, D. Stolten, J. Electrochem. Soc. **163**, F3197 (2016)
3. M. Shao, Q. Chang, J.-P. Dodelet, R. Chenitz, Chem. Rev. **116**, 3594 (2016)
4. X. Ge, A. Sumboja, D. Wuu, T. An, B. Li, F.W.T. Goh, T.S.A. Hor, Y. Zong, Z. Liu, ACS Catal. **5**, 4643 (2015)
5. A.R. Zeradjanin, J.P. Grote, G. Polymeros, K.J.J. Mayrhofer, Electroanalysis **28**, 2256 (2016)
6. P. Quaino, F. Juarez, E. Santos, W. Schmickler, J. Beilstein, Nanotechnology **5**, 846 (2014)
7. S. Cherevko, S. Geiger, O. Kasian, N. Kulyk, J.P. Grote, A. Savan, B.R. Shrestha, S. Merzlikin, B. Breitbach, A. Ludwig, K.J.J. Mayrhofer, Catal. Today **262**, 170 (2016)
8. I. Spanos, A.A. Auer, S. Neugebauer, X. Deng, H. Tüysüz, R. Schlögl, ACS Catal. **7**, 3768 (2017)
9. H.A. Miller, F. Vizza, M. Marelli, A. Zadick, L. Dubau, M. Chatenet, S. Geiger, S. Cherevko, H. Doan, R.K. Pavlicek, S. Mukerjee, D.R. Dekel, Nano Energy **33**, 293 (2017)
10. S. Cherevko, A.R. Zeradjanin, A.A. Topalov, N. Kulyk, I. Katsounaros, K.J.J. Mayrhofer, ChemCatChem **6**, 2219 (2014)
11. A.A. Topalov, S. Cherevko, A.R. Zeradjanin, J.C. Meier, I. Katsounaros, K.J.J. Mayrhofer, Chem. Sci. **631** (2014)
12. N. Hodnik, P. Jovanovič, A. Pavlišič, B. Jozinović, M. Zorko, M. Bele, V.S. Šelih, M. Šala, S. Hočevar, M. Gaberšček, J. Phys. Chem. C **119**, 10140 (2015)
13. P. Jovanovič, A. Pavlišič, V.S. Šelih, M. Šala, N. Hodnik, M. Bele, S. Hočevar, M. Gaberšček, ChemCatChem **6**, 449 (2014)
14. Z. Wang, E. Tada, A. Nishikata, Electrocatalysis **6**, 179 (2015)
15. S. Cherevko, A.R. Zeradjanin, G.P. Keeley, K.J.J. Mayrhofer, J. Electrochem. Soc. **161**, 822 (2014)
16. J.F. Llopis, J.M. Gamboa, L. Victori, Electrochim. Acta. **17**, 2225 (1972)
17. Y.M. Kolotyrkin, V.V. Losev, A.N. Chemodanov, Mater. Chem. Phys. **19**, 1 (1988)
18. V.S. Bagotzky, E.I. Khrushcheva, M.R. Tarasevich, N.A. Shumilova, J. Power Sources **8**, 301 (1982)
19. M. Pourbaix, *Atlas of electrochemical equilibria in aqueous solutions*, 2nd edn. (NACE International, Cecelcor, 1974)
20. S.O. Klemm, A.A. Topalov, C.A. Laska, K.J.J. Mayrhofer, Electrochem. Commun. **13**, 1533 (2011)
21. S. Cherevko, N. Kulyk, K. J. J. Mayrhofer, Nano Energy **1** (2015)
22. N. Kulyk, S. Cherevko, M. Auinger, C. Laska, K.J.J. Mayrhofer, J. Electrochem. Soc. **162**, H860 (2015)
23. N. Danilovic, R. Subbaraman, K.-C. Chang, S.H. Chang, Y.J. Kang, J. Snyder, A.P. Paulikas, D. Strmcnik, Y.-T. Kim, D. Myers, V.R. Stamenkovic, N.M. Markovic, J. Phys. Chem. Lett. **5**, 2474 (2014)
24. R. Kötz, H. Neff, S. Stucki, J. Electrochem. Soc. **131**, 72 (1984)
25. A. Minguzzi, O. Lugaresi, E. Achilli, C. Locatelli, A. Vertova, P. Ghignabc, S. Rondininiac, Chem. Sci. **5**, 3591 (2014)
26. H.G. Sanchez Casalongue, M.L. Ng, S. Kaya, D. Friebel, H. Ogasawara, A. Nilsson, Angew. Chem. **126**, 7297 (2014)
27. V. Pfeifer, T.E. Jones, J.J.V. Velez, C. Massue, M.T. Greiner, R. Arrigo, D. Teschner, F. Girgsdies, M. Scherzer, J. Allan, M. Hashagen, G. Weinberg, S. Piccinin, M. Haevecker, A. Knop-Gerickea, R. Schloegel, PCCP **18**, 2292 (2016)
28. M.E.G. Lyons, R.L. Doyle, I. Godwin, M.O. Brien, L. Russell, J. Electrochem. Soc. **159**, 932 (2012)
29. B.S. Yeo, A.T. Bell, J. Phys. Chem. C **116**, 8394–8400 (2012)
30. O. Diaz-Morales, D. Ferrus-Suspedra, M.T.M. Koper, Chem. Sci. **7**, 2639 (2016)
31. T. Binninger, R. Mohamed, K. Waltar, E. Fabbri, P. Levecque, R. Kötz, T.J. Schmidt, Sci. Rep. **1** (2015)